

# Bi-directional transportation of microagents induced by symmetry-broken acoustic streaming

Cite as: AIP Advances 9, 035352 (2019); <https://doi.org/10.1063/1.5089717>

Submitted: 22 January 2019 . Accepted: 21 March 2019 . Published Online: 29 March 2019

Sumit Mohanty , Ugo Siciliani de Cumis, Miguel Solsona, and Sarthak Misra



View Online



Export Citation



CrossMark



**Don't** let your writing keep you from getting published!

**AIP** | Author Services

Learn more today!

# Bi-directional transportation of micro-agents induced by symmetry-broken acoustic streaming

Cite as: AIP Advances 9, 035352 (2019); doi: 10.1063/1.5089717

Submitted: 22 January 2019 • Accepted: 21 March 2019 •

Published Online: 29 March 2019



Sumit Mohanty,<sup>1,a)</sup>  Ugo Siciliani de Cumis,<sup>1</sup> Miguel Solsona,<sup>2</sup> and Sarthak Misra<sup>1,3,b)</sup>

## AFFILIATIONS

<sup>1</sup>Surgical Robotics Laboratory, Department of Biomechanical Engineering, University of Twente, 7522NB Enschede, The Netherlands

<sup>2</sup>BIOS Lab-on-a-chip, University of Twente, 7522NH Enschede, The Netherlands

<sup>3</sup>Surgical Robotics Laboratory, Department of Biomedical Engineering, University Medical Centre Groningen, University of Groningen, 9713 AV Groningen, The Netherlands

<sup>a)</sup>Electronic mail: [s.mohanty@utwente.nl](mailto:s.mohanty@utwente.nl)

<sup>b)</sup>Electronic mail: [s.misra@utwente.nl](mailto:s.misra@utwente.nl)

## ABSTRACT

We show that vibrating protrusions inside a microchannel are capable of steering fluid away from their relative orientation. This phenomenon is brought forth by symmetry-broken design of these protrusions. Vibration of these asymmetric protrusions is reciprocated in the streaming effect at the boundary layers of the channel thus inducing a net fluid flow. Additionally, we show that the flow direction is sensitive to switching acoustic frequencies. This acoustically-induced flow has the potential for transportation of nanoparticles as well as complex micro-structures. We hereby demonstrate this utility for contactless actuation of flagellar micro-agents as a foreground towards targeted drug release.

© 2019 Author(s). All article content, except where otherwise noted, is licensed under a Creative Commons Attribution (CC BY) license (<http://creativecommons.org/licenses/by/4.0/>). <https://doi.org/10.1063/1.5089717>

Contactless manipulation of artificial and bio-hybrid micro-agents has emerged as an inter-disciplinary field of great interest, providing impetus to potential applications in life sciences.<sup>1</sup> Current state-of-the-art spans a plethora of contactless actuation mechanisms exploiting magnetism,<sup>1-7</sup> optics,<sup>8</sup> acoustics<sup>9-13</sup> and chemical principles.<sup>14</sup> The most ubiquitously employed method is micromanipulation with magnetic fields, which requires micro-agents to be magnetic. However, downsizing these agents further presents difficulty in fabricating them with sufficient magnetic volume.<sup>4,6,7</sup> Correspondingly, the induced magnetic forces are lower in comparison to the drag forces thereby making their standalone transport less effective. Alternatively, application of acoustics for micromanipulation has garnered attention owing to its clinical compliance<sup>15,16</sup> and complementarity to ultrasound imaging modality.<sup>17-20</sup> Traditionally, it has found usage in acoustic tweezers,<sup>21-23</sup> bubble-based cavitation<sup>10,24</sup> and actuation of mobile microswimmers.<sup>11,12</sup> Besides these, it has been notoriously capitalized for generating micro-vortices in confined microsystems premised upon the sound-fluid interaction.<sup>25-27</sup> This localized vorticing has been attributed to steady streaming generated

by oscillating sharp geometries, as these scatter sound waves into the surrounding fluid.<sup>27,28</sup>

An eclectic mix of microchannel designs have incorporated micro-structures on their side walls enabling boundary driven streaming to serve as micro-mixers<sup>27,29,30</sup> and transport of biological species.<sup>31,32</sup> Numerical investigations of these designs classify boundary-driven streaming as the causal force behind bulk streaming in these microchannels.<sup>27,33-35</sup> The most commonplace of these designs contain periodic arrays of sharp protrusions on their side walls, which upon their vibration exhibit symmetrical vorticing around them. This leads to equi-intensity counter-flowing fluxes around these protrusions, with no net displacement of fluid in the bulk of the channel thus making them suitable for mixing.<sup>27,30</sup> In contrast, by varying orientation of these protrusions it is possible to introduce an asymmetry which causes an imbalanced vorticing near the boundary layers, thus inducing a net flow.<sup>25</sup> Although the novelty of tilting the protrusions to generate flow has been demonstrated in the past,<sup>25,35</sup> the ability to control this flow with regards to excitation or design has not been explored yet. Moreover, this induced flow is accompanied with continuous displacement of

carrier fluid which is not always desirable for micromanipulation. On the other hand, while directional flow control by tuning excitation has been reported recently,<sup>36</sup> it is limited to low acoustic frequencies in sub-kHz range, thus providing scope for design compliant to higher frequencies.

In this study, we report that tilted microchannel protrusions are capable of producing a net flow in opposite direction relative to their orientation. This acoustically induced flow originates from dominant one sided vorticity around these protrusions due to asymmetric near boundary streaming around them as shown in Fig. 1(a). In addition, we establish that frequency-selective excitation of microchannels can induce a flow in both directions, complimentary to that reported previously.<sup>25</sup> This ability is also exploited for driving sperm-inspired artificial micro-swimmers inside the channel as depicted in Fig. 1(c). We fabricate our microchannels based on designs predicted by computational results and describe their actuation for certain characterized frequencies.

In order to prepare our microchannels, we followed the traditional PDMS (polydimethylsiloxane) based fabrication procedure by pouring a solution of PDMS mixed with curing agent (Sylgard 184) in 10:1 ratio over SU-8 molds of requisite design negatives on a Si wafer. The resulting single layer of cured PDMS was punched with inlets/outlets and plasma bonded over a glass substrate. We then glued a piezoelectric transducer (Pz27, Meggitt Ferroperm™) adjacent to the channel on the glass substrate using a two-component epoxy resin (Araldite, ARA400007) as shown in Fig. 1(b). This acted as our source of excitation which was interfaced with a signal generator (33510B, Keysight), while the acoustic power was further enhanced up to a maximum of 50V by a custom built high voltage amplifier (1MHz bandwidth).

We determined the operating frequencies of the transducer by performing its electro-mechanical characterization in subsequent steps. Since piezoelectrics harmonize to their resonant frequencies,<sup>37,38</sup> we measured the impedance spectrum of our transducer using an Impedance Analyzer (Agilent, HP4294A) for preliminary inspection of these frequencies as described in Fig. 1(d) and (e). We then measured vibration occurring at these frequencies in our workspace using Laser Doppler Vibrometer (Polytec, OFV-5000) on the surface of transducer, and compared them with that on the

glass substrate close to the transducer as shown in Fig. 1(f). This dual confirmation was necessary as resonant harmonics of piezoelectrics could potentially shift due to acoustic loading.<sup>38–40</sup> Moreover, the relative strength of vibrations also provided a suitable operating range to ensure sufficient acoustic power transmission to our workspace.

The physics behind generating a directional flow was conceived from computational modeling of acoustic streaming, as investigated in several reports.<sup>27,28,30,33,34</sup> It has been notoriously described as steady flow generated as fluid's inertial reaction to absorption of sound waves, occurring predominantly at physical boundaries.<sup>27,28,30</sup> A common strategy to simplify its computation is by separating the time-scales of sound propagation through the medium and fluid's response to it.<sup>27,34,41</sup> Going by this principle, we defined our study based on the boundary conditions and governing formulations comprehensively described by Muller *et al.*<sup>34</sup> In this approach, we performed simulations (COMSOL Multiphysics™) on a parametric variation of microchannel designs, which worked as our computational domain to study the influence of different geometrical parameters. We simulated our designs with the intuitive notion that tilting their side-wall protrusions could effectively orient the steady flow, while varying the channel width could influence the region where it occurs. For any given orientation of protrusions across the channel, the overall flow profile is oscillatory but as they come closer, a steady offset appears in the middle of the channel. This offset corresponds to a steady flow of the fluid in the direction pointed by the protrusions. We denote this case as *forward* flow. However, when the separation across the channel increases, the steady flow develops in the opposite direction to their orientation, a case that we define as *reverse* flow. This happens when protrusions across the channel are far enough allowing the boundary-driven streaming to attenuate sufficiently and thereby sustain a steady flow in the middle of the channel as shown in Fig. 2(c). Further, to homogenize our framework, we simulated the channel described in Fig. 1(a) at a constant acoustic excitation frequency of 50kHz. Thus, for this frequency, Fig. 2(a) represents the flow profile of two contrasting observations described above for two different channel widths. Additionally, to effect eliminate the influence of geometry, we varied the protrusion angle ( $\alpha$ ) and channel width ( $W$ ) in

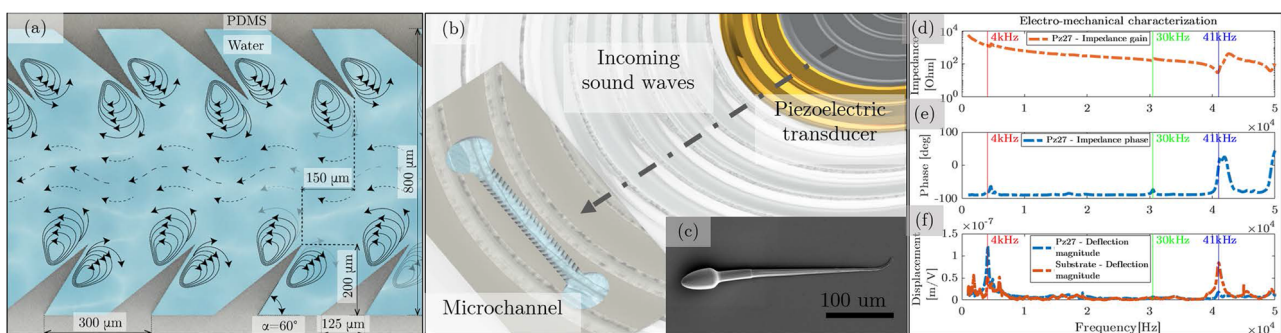


**FIG. 1.** (a) An illustration of symmetry-broken acoustic streaming around microchannel protrusions. (b) Schematic of the workspace describing wave propagation. (c) A micrograph of sperm inspired micro-swimmer used for experiments. Electro-mechanical evaluation of harmonic modes of transducer (Pz27, Meggitt Ferroperm™): (d) and (e) Impedance characteristics of transducer, with isolated the resonant harmonics marked by the characteristic impedance dip and phase jump at corresponding frequencies. (f) Mechanical deflections measured by the vibrometer (normalized over a distribution of 9 points on the transducer) for the frequency range depicted in (d) and (e).

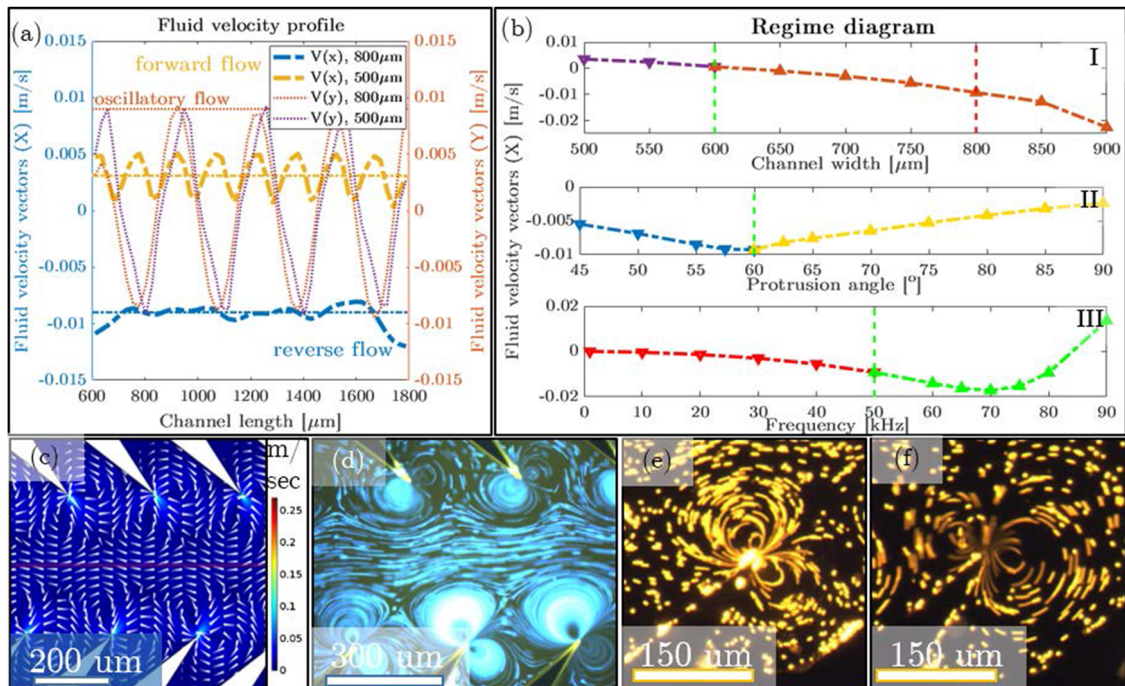


**FIG. 2.** (a-c) Summary of simulation study: (c) A close-up of simulated fluid velocity profile across the channel (described in Fig. 1(a)). The white arrows depict the streaming direction and fluid velocities are further resolved into  $v_x$  and  $v_y$  components, which are analyzed along a central parting line (in red). (a) A comparative fluid flow profile for two channel designs of width 800  $\mu\text{m}$  and 500  $\mu\text{m}$ . For similar magnitudes of oscillatory  $v_y$  component, the two channels exhibit a contrasting flow profile with  $v_x$  having a positive offset in case of 500  $\mu\text{m}$ , and a negative offset for the 800  $\mu\text{m}$  wide channel. The two flow regimes are indicated with arrows. (b) Regime diagram of  $v_x$  and  $v_y$  for the parametric study based on design variations with respect to (I) channel width,  $W$  (at 50kHz), (II) protrusion angle,  $\alpha$  (at 50kHz) and (III) frequency of acoustic excitation ( $W=800\mu\text{m}$ ,  $\alpha=60^\circ$ ). (d) Time-lapse image illustrating *reverse flow* observed with blue fluorescent tracer particles,  $W=800\mu\text{m}$ . (e-f) Frequency-based bi-directionality observed with yellow fluorescent tracer particles illustrating: (e) Reverse flow at 41kHz and (f) Forward flow at 4kHz. Multimedia views: (d) <https://doi.org/10.1063/1.5089717.1>; [(e) and (f)]: <https://doi.org/10.1063/1.5089717.2>.

Fig. 1(a) separately, keeping other parameters constant. We summarize our findings in a regime diagram shown in Fig. 2(b) to find the optimal channel design to establish *reverse flow*. Firstly, we observe a crossover region for  $W=600\mu\text{m}$  where the flow switches from *forward* to *reverse* regime for wider channels as shown in Fig. 2(b)–I. Secondly, in Fig. 2(b)–II we observe that for  $W=800\mu\text{m}$ , tilting the protrusions beyond a threshold ( $\alpha=60^\circ$ ) decreases the *reverse flow* magnitude. Although it wasn't possible to perform these simulations for varying frequencies owing to computational limitations, we narrowed down to a lower frequency range as shown in Fig. 2(b)–III. For the design in Fig. 1(a) (i.e.  $W=800\mu\text{m}$ ,  $\alpha=60^\circ$ ), it was observed that the *reverse flow* component increases with frequency up to a threshold beyond which it decreases.

In order to gain deeper understanding of the simulations, we performed experiments to test the directional flow inside the microchannel referred to in Fig. 1(a) for two different widths i.e. 600  $\mu\text{m}$  and 800  $\mu\text{m}$ . Firstly, in case of 800  $\mu\text{m}$  wide channel, we excited an aqueous solution of fluorescent particles (2.5  $\mu\text{m}$  blue alignment beads, Alignflow™) in this channel to an operating frequency of 41kHz, subjecting them to varying acoustic power (Fig. 2(d), Video 1, Multimedia view). At low power we observed a *forward flow* close to the protrusions, while the central region away from them exhibits a *reverse flow* which further intensified

as we gradually increased the power. Similarly, we excited the blue tracer particles in 600  $\mu\text{m}$  wide channel at 41kHz and observed that the *reverse flow* prevails but in a much narrower region (Video 1, Multimedia view). This is in agreement with the crossover regime observed in Fig. 2(b). Further, to test the influence of acoustic wavelength on the behavior of this flow, we operated the channel to frequencies characterized earlier in Fig. 1(d)–(f). As can be seen in Fig. 2(f) (Multimedia view), we began by exciting particles (2.5  $\mu\text{m}$  yellow alignment beads, Alignflow™) to a frequency of 4kHz to observe a predominantly *forward flow*, extending throughout the channel. When the excitation was turned off, a strong back-flow of water suggested a net displaced liquid. This abides with a similar observation reporting pumping functionality of microchannel at 6.5kHz.<sup>25</sup> Whereas exciting the channel to higher frequencies of 30kHz and 41kHz, resulted in a *reverse flow* in the middle of the channel as was also observed by the general trend in regime diagram around these frequencies as shown in Fig. 2(b). Although the flow observed for the case of 30kHz was much lower, this conformed to the lower acoustic power at this frequency as observed earlier in Fig. 1(f). However, there was a significant *reverse flow* observed at 41kHz in the bulk of the channel. This could also be related to the fact that sound waves attenuate at shorter distances for higher frequencies thus confining their boundary-driven streaming.<sup>42</sup>

Secondly, we also observe that the relative size of counter-rotating vortices differ for 4kHz and 41kHz as can be seen in Fig. 2(e) and (f) (Multimedia view). In case of 4kHz, the lower vortex is larger and clockwise thus pulling the fluid along the protrusions. While for the 41kHz case, the upper vortex is larger and counter-clockwise pushing the water away from the protrusions. Moreover, the limited back-flow of water for higher frequencies was in contrast to the pumping utility referred to earlier,<sup>25</sup> as despite of the *reverse* flow observed in the bulk, the *forward* flow around the protrusions conserved the net flow. Hence, operating the channel under *reverse* flow conditions was considered more suitable for micromanipulation due to its ability to generate a confined flow with little displacement of fluid.

Thereon, we investigated the utility of these two flow regimes through manipulation of micro-swimmers. We first performed a preliminary test where we stained PDMS fragments of roughly 100 $\mu\text{m}$  size with blue fluorescent particles and injected them into the channel. Fig. 3(a) (Video 3, Multimedia view) captures trail of a dyed PDMS fragment traversing along the *reverse* flow in the channel when excited at 41kHz. We subsequently performed experiments with our sperm-inspired swimmer of length 100 $\mu\text{m}$  in the presence of tracer particles. It has been reported previously that streaming

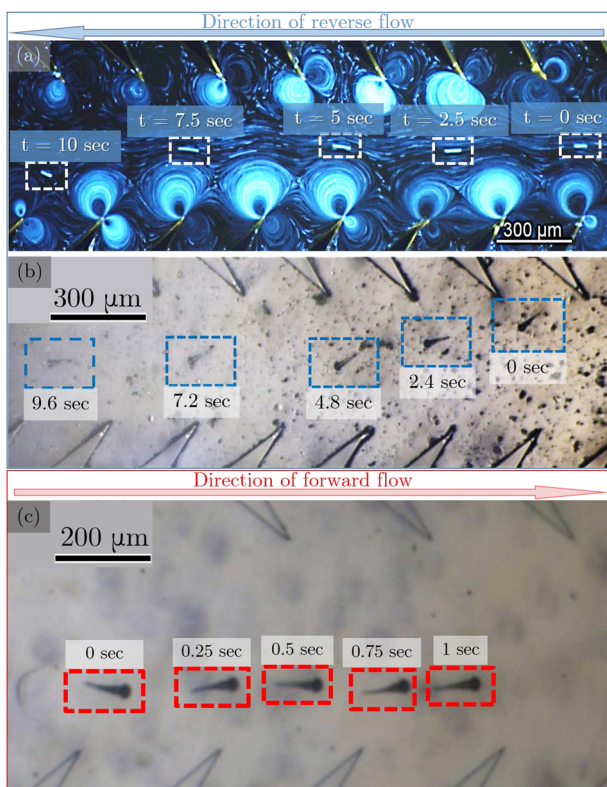


**FIG. 3.** Time-lapse sequence showing motion of micro-agents in the microchannel to acoustic excitation. (a) A dyed PDMS fragment (*inscribed in white box*) at a frequency of 41kHz. (b) A sperm-inspired swimmer (*inscribed in box*) to a frequency of (b) 41kHz and (c) 4kHz. Multimedia views: <https://doi.org/10.1063/1.5089717.3>; <https://doi.org/10.1063/1.5089717.4>; <https://doi.org/10.1063/1.5089717.5>.

fluxes around the flagellar appendages of micro-structures can trigger a beating motion thereby causing them to swim.<sup>11-13</sup> We thus based our micro-swimmers on a sperm-inspired design as shown in Fig. 1(c). Our micro-swimmers were made of IPL-780 (Nanoscribe GmbH) and fabricated using Direct Laser Writing technique.<sup>4,7</sup> Firstly, a 100 $\mu\text{m}$  swimmer was injected into the channel, which was excited at 41kHz, whose motion is described in Fig. 3(b) (Video 4, Multimedia view). Contrary to the previous observation, the drift caused by acoustically induced flow occurs in tandem with the flagellar beating which helps the swimmer to steer through the channel. Further, we excited a 100 $\mu\text{m}$  swimmer at 4kHz under *forward* flow conditions, as can be seen in Fig. 3(c) (Video 5, Multimedia view). The flagellum here exhibits stronger beating as being close to the protrusions where the oscillatory flow is dominant.

In conclusion, we demonstrate a unique phenomenon where acoustically exciting protrusions in a microchannel generates a flow opposite to their relative orientation, which we denote here as *reverse* flow. Additionally, we demonstrate that this *reverse* flow in the middle of the channel occurs in tandem with *forward* flow close to the protrusions which conserves the net flow. We use a simplistic approach to computationally model the governing acoustofluidics to find suitable design metrics for constructing our channel. In the future, this study could incorporate geometrically more complex designs of side wall protrusions to produce the same effect. We further experimentally observe *reverse* flow to dominantly occur at high frequencies, and the *forward* flow at just below ultrasound range. This also makes the *reverse* flow regime more convenient for operation at higher power as the frequencies lie in inaudible range for human hearing. Improving the tunability of designs with respect to acoustic frequencies could accommodate more operating points for *forward* flow regime. Finally, we exploit this effect for micromanipulation within the channel, which can be useful for applications requiring contactless delivery of micro-agents. Deeper understanding and control of their acoustic excitation can provide scope for maneuvering them by multiplexing between the variable flow regimes.

This work was supported by funds from The Netherlands Organization for Scientific Research (Innovational Research Incentives Scheme-VICI: SAMURAI project #14855). We would like to thank Remco Sanders and Huib van Vossen for their advice on characterization and microfabrication. We would also like to thank Paul ter Braak and Vasilis Papadimitriou for their help with fluorescence imaging.

## REFERENCES

- B. J. Nelson, I. K. Kaliaktsos, and J. J. Abbott, *Annual Review of Biomedical Engineering* **12**, 55 (2010).
- L. Zhang, J. J. Abbott, L. Dong, B. E. Kratochvil, D. Bell, and B. J. Nelson, *Applied Physics Letters* **94** (2009).
- L. Zhang, K. E. Peyer, and B. J. Nelson, *Lab on a Chip* **10**, 2203 (2010).
- S. Tottori, L. Zhang, F. Qiu, K. K. Krawczyk, A. Franco-Obregon, and B. J. Nelson, *Advanced Materials* **24**, 811 (2012).
- R. W. Carlsen, M. R. Edwards, J. Zhuang, C. Pacoret, and M. Sitti, *Lab on a Chip* **14**, 3850 (2014).
- I. S. Khalil, H. C. Dijkstra, L. Abelmann, and S. Misra, *Applied Physics Letters* **104** (2014).
- S. Kim, S. Lee, J. Lee, B. J. Nelson, L. Zhang, and H. Choi, *Scientific Reports* **6** (2016).

- <sup>8</sup>E. Avci, M. Grammatikopoulou, and G. Z. Yang, *Advanced Optical Materials* **5** (2017).
- <sup>9</sup>A. Marzo, S. A. Seah, B. W. Drinkwater, D. R. Sahoo, B. Long, and S. Subramanian, *Nature Communications* **6** (2015).
- <sup>10</sup>D. Ahmed, M. Lu, A. Nourhani, P. E. Lammert, Z. Stratton, H. S. Muddana, V. H. Crespi, and T. J. Huang, *Scientific Reports* **5** (2015).
- <sup>11</sup>D. Ahmed, T. Baasch, B. Jang, S. Pane, J. Dual, and B. J. Nelson, *Nano Letters* **16**, 4968 (2016).
- <sup>12</sup>M. Kaynak, A. Ozcelik, A. Nourhani, P. E. Lammert, V. H. Crespi, and T. J. Huang, *Lab Chip* **17**, 395 (2017).
- <sup>13</sup>M. Kaynak, A. Ozcelik, N. Nama, A. Nourhani, P. E. Lammert, V. H. Crespi, and T. J. Huang, *Lab on a Chip* **16**, 3532 (2016).
- <sup>14</sup>I. S. M. Khalil, V. Magdanz, S. Sanchez, O. G. Schmidt, and S. Misra, *PLoS One* **9** (2014).
- <sup>15</sup>D. Mark, S. Haeberle, G. Roth, F. von Stetten, and R. Zengerle, *Chemical Society Reviews* **39**, 1153 (2010).
- <sup>16</sup>D. Das, K. Sivasubramanian, C. Yang, and M. Pramanik, *Scientific Reports* **8** (2018).
- <sup>17</sup>M. Wiklund, R. Green, and M. Ohlin, "Acoustofluidics 14: Applications of acoustic streaming in microfluidic devices" (2012).
- <sup>18</sup>T. Segers, N. de Jong, D. Lohse, and M. Versluis, *Microfluidics for Medical applications* (Royal Society of Chemistry, 2014), pp. 81–101.
- <sup>19</sup>S. A. Peyman, J. R. McLaughlan, R. H. Abou-Saleh, G. Marston, B. R. Johnson, S. Freear, P. L. Coletta, A. F. Markham, and S. D. Evans, *Lab on a Chip* **16**, 679 (2016).
- <sup>20</sup>H. Lin, J. Chen, and C. Chen, "A novel technology: microfluidic devices for microbubble ultrasound contrast agent generation" (2016).
- <sup>21</sup>J. Shi, D. Ahmed, X. Mao, S. C. S. Lin, A. Lawit, and T. J. Huang, *Lab on a Chip* **9**, 2890 (2009).
- <sup>22</sup>F. Guo, Y. Xie, S. Li, J. Lata, L. Ren, Z. Mao, B. Ren, M. Wu, A. Ozcelik, and T. J. Huang, *Lab on a Chip* **15**, 4517 (2015).
- <sup>23</sup>F. Guo, Z. Mao, Y. Chen, Z. Xie, J. P. Lata, P. Li, L. Ren, J. Liu, J. Yang, M. Dao, S. Suresh, and T. J. Huang, *Proceedings of the National Academy of Sciences* **113**, 1522 (2016).
- <sup>24</sup>D. Ahmed, C. Dillinger, A. Hong, and B. J. Nelson, *Advanced Materials Technologies* **2** (2017).
- <sup>25</sup>P. H. Huang, N. Nama, Z. Mao, P. Li, J. Rufo, Y. Chen, Y. Xie, C. H. Wei, L. Wang, and T. J. Huang, *Lab on a Chip* **14**, 4319 (2014).
- <sup>26</sup>D. J. Collins, B. L. Khoo, Z. Ma, A. Winkler, R. Weser, H. Schmidt, J. Han, and Y. Ai, *Lab on a Chip* **17**, 1769 (2017).
- <sup>27</sup>N. Nama, P.-H. Huang, T. J. Huang, and F. Costanzo, *Lab on a Chip* **14**, 2824 (2014).
- <sup>28</sup>M. Ovchinnikov, J. Zhou, and S. Yalamanchili, *The Journal of the Acoustical Society of America* **136**, 22 (2014).
- <sup>29</sup>D. Ahmed, X. Mao, J. Shi, B. K. Juluri, and T. J. Huang, *Lab on a Chip* **9**, 2738 (2009).
- <sup>30</sup>P.-H. Huang, Y. Xie, D. Ahmed, J. Rufo, N. Nama, Y. Chen, C. Y. Chan, and T. J. Huang, *Lab on a Chip* **13**, 3847 (2013).
- <sup>31</sup>D. Ahmed, A. Ozcelik, N. Bojanala, N. Nama, A. Upadhyay, Y. Chen, W. Hanna-Rose, and T. J. Huang, *Nat Commun* **7**, 1 (2016).
- <sup>32</sup>N. Läubli, N. Shamsudhin, D. Ahmed, and B. J. Nelson, *Procedia CIRP* **65**, 93–98 (2017).
- <sup>33</sup>A. Lamprecht, "Optical traps for characterising acoustically induced forces and torques acting on microparticles," Ph.D. thesis, ETH Zurich (2017).
- <sup>34</sup>P. B. Muller, R. Barnkob, M. J. H. Jensen, and H. Bruus, *Lab on a Chip* **12**, 4617 (2012).
- <sup>35</sup>L. Feng, B. Song, D. Zhang, Y. Jiang, and F. Arai, *Micromachines* **9**, 596 (2018).
- <sup>36</sup>R. Jain and B. Lutz, *Lab on a Chip* **17**, 1552 (2017).
- <sup>37</sup>J. Dual, P. Hahn, I. Leibacher, D. Möller, and T. Schwarz, *Lab on a Chip* **12**, 852 (2012).
- <sup>38</sup>N. Pérez, F. Buiochi, M. A. B. Andrade, and J. C. Adamowski, "Numerical characterization of piezoceramics using resonance curves" (2016).
- <sup>39</sup>Y. R. Wong, H. Du, and X. Pang, *NDT and E International* **76**, 61 (2015).
- <sup>40</sup>F. J. Arnold, L. L. B. Roger, M. S. Gonçalves, and S. S. Mühlen, *Ecti Transactions on Electrical Eng., Electronics, and Communications* **12**, 48 (2014).
- <sup>41</sup>J. Lei, P. Glynn-Jones, and M. Hill, *Microfluidics and Nanofluidics* **21** (2017).
- <sup>42</sup>M. B. Dentry, L. Y. Yeo, and J. R. Friend, *Physical Review E - Statistical, Nonlinear, and Soft Matter Physics* **89** (2014).